Available online at www.sciencedirect.com
SCIENCE DIRECT®
Journal of Magnetic Resonance 175 (2005) 44–51
JMR Journal of Magnetic Resonance
www.elsevier.com/locate/jmr

# Rapid-scan EPR with triangular scans and fourier deconvolution to recover the slow-scan spectrum

Janhavi P. Joshi, John R. Ballard, George A. Rinard, Richard W. Quine, Sandra S. Eaton *, Gareth R. Eaton

*Department of Chemistry and Biochemistry, University of Denver, Denver, CO 80208, USA*
*Department of Engineering, University of Denver, Denver, CO 80208, USA*

Received 12 January 2005; revised 17 March 2005
Available online 14 April 2005

**Abstract**

Direct-detected rapid-scan EPR signals were recorded using triangular field scan rates between 1.7 and 150 kG/s for deoxygenated samples of lithium phthalocyanine (LiPc) and Nycomed trityl-$CD_3$. These scan rates are rapid relative to the reciprocals of the electron spin relaxation times and cause characteristic oscillations in the signals. Fourier deconvolution with an analytical function permitted recovery of lineshapes that are in good agreement with experimental slow-scan spectra. Unlike slow-scan EPR, direct detection rapid-scan EPR does not use phase sensitive detection and records the absorption signal directly instead of the first derivative of the absorption signal. The amplitude of the signal decreases approximately linearly with applied magnetic field gradient. Images of phantoms constructed from samples of LiPc and trityl-$CD_3$ were reconstructed by filtered back-projection from data sets with a missing angle. The lineshapes in spectral slices from the image are in good agreement with slow-scan spectra and the spacing between sample tubes matches well with the known sample geometry.


## 1. Introduction

Early in the development of NMR, transient effects, called "wiggles," were observed after the magnetic field passed through resonance in a time that was short relative to $T_1$ and $T_2$ [1,2]. Since inhomogeneity over the sample causes the oscillations to damp out more rapidly, this effect was used in CW NMR to guide the shimming of the magnetic field to maximum homogeneity. It was shown that the slow-scan NMR spectra could be recovered from rapid-scan signals by deconvolution or cross-correlation, using either a standard experimental response [3–5] or an analytic function [6–8]. This technique was called "Correlation NMR Spectroscopy," or "Rapid-Scan Fourier Transform NMR Spectroscopy." Rapid-scan NMR achieved almost as high a signal-to-noise, per unit time, for proton spectra of simple organic molecules in fluid solution as could be achieved by pulsed FT-NMR. For example, with $T_1$ equal to 1 s and a full spectral scan in four $T_1$, correlation spectroscopy was only 35% less sensitive than a pulsed FT experiment acquired with a period of three $T_2$ [9]. Correlation NMR was used to measure nuclear relaxation times [8,10,11] and for solvent peak suppression [10,12,13]. Methods to optimize rapid-scan NMR data processing have been discussed [7,14–16]. Rapid scan looked very promising in the early 1970s, but was soon eclipsed by FT-NMR due to the wide range of pulse sequences that became available [9,17]. Correction of a spectrum using deconvolution with a distorted reference signal has subsequently been used in other NMR experiments [18].

Background literature on adiabatic rapid-passage EPR is discussed in [19]. Only a few examples of rapid-scan EPR have been reported. Rengen et al. [20] considered the rates of magnetic field scan at which

* Corresponding author. Fax: +1 303 871 2254.
*E-mail address:* seaton@du.edu (S.S. Eaton).

1090-7807/$ - see front matter © 2005 Elsevier Inc. All rights reserved.
doi:10.1016/j.jmr.2005.03.013

passage effects and detector filter bandwidth effects would distort a rapid-scan EPR signal. The oscillations following a rapid-scan EPR signal were observed by Czoch et al. [21]. EPR signals at 250 MHz for a single crystal of lithium phthalocyanine (LiPc) in the absence of oxygen and for a deoxygenated aqueous solution of Nycomed trityl-$CD_3$ radical were recorded at scan rates between $1.3 \times 10^3$ G/s and $3.4 \times 10^5$ G/s in the center of sinusoidal scans [19]. LiPc and trityl-$CD_3$ were selected for our initial studies because of the utility for in vivo EPR imaging of samples with narrow-line EPR signals. These initial experiments were performed using the field modulation module of the Bruker Elexsys console to generate sinusoidal magnetic field scans. Direct detection of the signal with a double balanced mixer was used to record the absorption signal, instead of the usual phase sensitive detection at the modulation frequency which gives the first derivative [19]. These experiments provided the first systematic characterization of direct-detected rapid-scan EPR signals. Subsequent experiments demonstrated the impact on X-band rapid-scan signals of resonator $Q$ and inhomogeneous broadening due to eddy currents in the resonator [22].

A disadvantage of the sinusoidal scans is that the scan rate varies continuously across the scan. To recover the slow-scan spectrum from rapid-scan data, it is advantageous to have a linear scan rate (triangular scan) so that the scan rate remains constant across each half-cycle of the scan. For this purpose we have constructed a system that generates triangular field scans with scan frequencies between 1 and 10 kHz and scan widths of 1–10 G. Results obtained at 250 MHz with triangular scans and Fourier deconvolution to recover the slow-scan spectrum are described here.

## 2. Experimental

### 2.1. Samples

LiPc prepared electrochemically following procedures in the literature [23,24] was provided by Prof. Swartz, Dartmouth University. Well-shaped needles were selected, placed in 4 mm OD quartz tubes, and evacuated overnight on a high vacuum line, and then the tubes were flame sealed. Solutions (0.2 or 0.5 mM) of Nycomed trityl-$CD_3$ (methyltris(8-carboxy-2,2,6,6-tetramethyl($d_3$)-benzo[1,2-d:4,5-d′]bis(1,3)dithiol-4-yl) tri potassium salt) in water in 4 mm OD quartz tubes or 10 mm OD pyrex tubes were bubbled extensively with $N_2$ gas to remove oxygen and then flame sealed.

### 2.2. Spectroscopy

Rapid-scan signals at 250 MHz were obtained on a locally designed and built spectrometer [25] that includes a Bruker E540 console, which was used to control the dc field and the Bruker magnetic-field gradient power supplies. Rapid-scan data were acquired using the pulse signal pathway in the locally designed bridge [25] and digitized using the Bruker SpecJet. Acquisition of quadrature data permitted optimization of signal phasing by post-processing and complex Fourier deconvolution of the signals. The low-pass single-pole filter bandwidth of 5 MHz in the signal channel of the locally designed bridge was used.

### 2.3. Magnets, gradient coils, resonators, and scan coils

Two assemblies were used in the experiments:

*Assembly (I)*. This configuration used an air-core magnet with four equal diameter (40 cm) coils [25]. Magnetic field gradients in the $Z$-direction (the direction of the dc field) were generated with a pair of 17-cm average diameter coils spaced 18 cm apart. The gradient coils were calibrated using a phantom consisting of two LiPc samples separated by 1.5 mm; the gradient coil constant was 2.3 G/cm/A. To control the field the Bruker Hall probe was positioned approximately in the nodal plane of the gradient. The offset in center field as a function of gradient was determined and the correction applied to data files.

With this magnet assembly the same 5-turn resonator as described in [19] was used, but with a different shield. The resonator was constructed from no. 16 copper wire and had an internal diameter of about 4.3 mm. The modified shield was constructed from 0.025 mm thick brass sheet supported externally by epoxy impregnated glass cloth. The shield was 5.5 cm high with a diameter of 4 cm. This shield allowed good penetration of the rapid-scan magnetic field. The $Q$ of this resonator, measured using a HP8753D network analyzer, was ~160. The resonator efficiency $(B_1/\sqrt{P})$ was $5.5 \pm 0.5$ G/$\sqrt{\text{Watt}}$ [19]. This resonator is referred to as the 4 mm multi-turn resonator.

Rapid magnetic field scans were generated with 17 cm diameter Helmholtz scan coils that also were used for magnetic field modulation with phase sensitive detection of slow-scan spectra. Calibration based on the peak-to-peak linewidths in slow-scan first-derivative LiPc spectra recorded using phase sensitive detection at the modulation frequency gave a scan coil constant of $7.3 \pm 0.5$ G/A.

*Assembly (II)*. This configuration used an 81 cm diameter four-coil air-core magnet designed for good side access and a pair of $Z$-gradient (Maxwell) coils with an outer diameter of 49 cm, spaced 30 cm apart [26]. The calibrated gradient produced by these coils was 0.56 G/cm/A. To use the Bruker Hall probe field control system, but avoid interaction with the gradients, the Hall probe was located in an auxiliary magnet coil system connected in series with the main magnet. This was

analogous to the configuration that was described previously [26]. To allow setting of the dc magnetic field with 10 times greater resolution than is available in the Bruker software at the low magnetic fields required for these experiments, the auxiliary magnet system had a coil constant 10 times greater than the magnet that was used for the experiments.

For this assembly a resonator constructed from 6 equally spaced turns of no. 20 copper wire was used. The resonator has an internal diameter of 25 mm and height of 50 mm. The spacing between the turns is 10 mm. A Voltronics, 25 series, non-magnetic, porcelain chip capacitor was connected in series between each turn of the coil. The resonator frequency was tuned using a combination of 10 and 3.7 pF capacitors. The $Q$ of the empty resonator was measured to be $155 \pm 5$. The resonator efficiency $(B_1/\sqrt{P})$ was determined to be $0.35 \pm 0.05$ G/$\sqrt{\text{Watt}}$ by comparing the calculated and experimental power saturation curves for 0.2 mM trityl-$CD_3$ obtained using both phase-sensitive detected slow-scans and direct-detected rapid-scans. This resonator is referred to as the 25 mm multi-turn resonator.

The scan coil assembly was a direct geometric scale model of the four-coil magnet system, with a large coil diameter of 10 cm. The resonator and the scan coil assembly were shielded using a non-magnetic stainless steel stock pot (Shopko, Longmont, CO) that is 33 cm in diameter and 26 cm high. Electrical contact between the pot and its cover was achieved with finger-stock. Having the shield outside the scan coils helps to eliminate field inhomogeneities produced by the eddy currents that are observed when the shield is between the scan coils and the resonator [19,22]. Calibration of the scan widths, by the method described for the 17 cm diameter Helmholtz scan coils, gave a field constant of $10.8 \pm 0.2$ G/A.

### 2.4. Triangular scans

The triangle current driver that was used for these studies is a preliminary version that was designed to test the approach. It is a power amplifier based on the Apex Microtechnology (Tucson, Arizona) PB-58A power booster op-amp. This device has a current dynamic range of $\pm 1.5$ A and a voltage range of about $\pm 135$ V at its output. It is incorporated into a closed loop system that accepts an input voltage (supplied by an HP model 3310B function generator) as a current reference. The closed loop configuration with a high gain error amplifier converts any input waveform into a corresponding current waveform in the coils, within the bandwidth and dynamic range limits of the system. The transfer function of the driver is 1 A/V. The tests described below show linear current scans up to a 10 kHz triangle frequency with some rounding of the waveform peaks at the highest frequencies due to the bandwidth limits of the power amplifier, which attenuates the higher harmonic response. This driver has been used with several different sets of rapid-scan coils, and the only change required from one coil set to another is to retune the loop compensation network for the different inductances of the coils.

Rapid-scan signals were recorded with scan frequencies in the range of 1–10 kHz and scan widths in the range of 0.64–9.72 G. The RF power levels were selected such that the response of the spin system was linear. The incident RF power on the resonator at 0 dB is 43 mW. In experiments with the trityl radical in the 4 mm multi-turn resonator, an RF power of 45 dB ($B_1 = 6.4$ mG) was used. In the experiments with the 25 mm multi-turn resonator, an RF power of 26 dB ($B_1 = 3.6$ mG) was used.

### 2.5. Simulations of rapid-scan signals

Simulations were performed by numerical integration of the rotating-frame representation of the Bloch equations using a program written in Compaq Visual Fortran 6.5 [19]. The original program [19], which was written to simulate signals acquired using sinusoidal scans, was modified to simulate signals recorded using triangular scans. The spin–lattice relaxation time ($T_1$) and the spin–spin relaxation time ($T_2$) measured by inversion recovery and two pulse spin echo, respectively, were constants in the simulations. For trityl $T_1 = 11.5$ μs and $T_2 = 8$ μs and for LiPc $T_1 = 3.5$ μs and $T_2 = 2.5$ μs at 250 MHz [19]. The resonator $Q$ and the bridge filter bandwidth of 5 MHz also were fixed parameters in the simulations. The scan frequency was set to the experimental value. To calibrate the relationship between current through the scan coils and scan widths, the scan width was adjusted to match the calculated lineshape to the experimental lineshape. Thereafter the calibrated scan widths were input to the simulations. The inhomogeneously broadened lineshapes were modeled as the sum of contributions from $T_2$-determined spin packets with differing offsets from the center of the signal. Simulations of the trityl and LiPc signals used 47 and 20 spin packets, respectively. The weightings of the spin packets in the distribution were calculated using an approximation for a Voigt function [27]. The inhomogeneous broadening described by the half-width at half-height of the distribution was adjusted to account for the magnetic field inhomogeneities that affect the rate of damping of the rapid-scan signals. For scan rates in the range of 1.76–104 kG/s the inhomogeneous broadening was 14–26 mG for a trityl sample in a 4 mm OD tube in the 4 mm multi-turn resonator and 12–16 mG for a trityl sample in a 10 mm OD tube in the 25 mm multi-turn resonator. The smaller inhomogeneous broadening over a larger sample volume in Assembly II indicates that positioning the shield outside the scan coils had the desired effect of decreasing the eddy cur-

rents. In the case of trityl signals the lineshape included the $^{13}C$ sidebands with hyperfine splitting of 0.166 G.

### 2.6. Testing the linearity of the triangular scan

The shape of the rapid-scan signal depends sensitively on scan rate. By simulating the rapid-scan signals using a linear scan rate and comparing it to the experimental signal, the linearity of the experimental scan rate can be determined. Thus, the rapid-scan signal shape was used as a probe to detect deviations in the linearity of the triangular scan. The tests were performed at various scan widths and scan frequencies with the 4 mm multi-turn resonator and $B_1 = 6.4$ mG. The linearity of the scan also was checked by comparing the positions of $^{13}C$ sidebands in the rapid-scan trityl spectrum with the hyperfine splittings measured in an X-band CW spectrum recorded using a Bruker E580 spectrometer.

### 2.7. Deconvolution of the rapid-scan signals

The rapid-scan experimental conditions can be viewed as a driving function $a(t)$ that acts upon a spin system for which the slow-scan spectrum is $s(t)$, to produce a rapid-scan signal $o(t)$. The output power and frequency, $\omega$, of the RF source are constant. The magnetic field, $B_0$, is swept, so the difference frequency, $\omega_0 - \omega$, between the electron spin resonance frequency, $\omega_0 = (g\beta/\hbar)B_0$, and the source frequency varies linearly with time. The time-dependent driving function $a(t) = \exp(ibt^2/2)$, where $b$ is the scan rate, represents the linearly varying scan of $\omega_0 = bt$. [6]. For these EPR experiments $b = 2(g\beta/h)B_m(2\pi v_m)$ rad/s$^2$, where $g\beta/h$ is the conversion factor from Gauss to Hz, $B_m$ is the scan width in Gauss, $2\pi v_m$ is the angular scan frequency and the additional factor of 2 takes account of the fact that the field passes through resonance twice in each cycle of the triangular scan. If the rapid-scan experimental conditions are in the linear region, then $o(t) = a(t) * s(t)$ where $*$ is the linear convolution operator. Deconvolution of the rapid-scan signal to obtain the corresponding slow-scan spectrum is facilitated by taking the reverse Fourier transform such that $O(\omega) = A(\omega)S(\omega)$. After this reverse transformation the convolution becomes a simple multiplication and the transform of the slow-scan spectrum $S(\omega) = O(\omega)/A(\omega)$. $A(\omega) = \exp(-i\omega^2/2b)$ [6], which is the analytic function that was used for the deconvolution. Fourier transformation of $S(\omega)$ gives the desired slow-scan spectrum. Data were acquired with the following phase convention: the absorption signal has positive amplitude and the dispersion signal has its negative excursion prior to the positive excursion. The starting points of the half-cycles were determined by digitization of the triangular waveform output from the current driver and identification of maxima and minima in the waveform. The complex experimental arrays were zero-filled to a length of 8192 points prior to Fourier transformation. The lineshape of the deconvolved spectrum is quite sensitive to the phase of the original data. Imperfect phasing of the experimental data was corrected manually.

### 2.8. Testing of the deconvolution procedure

Rapid-scan signals of LiPc recorded using the 25 mm multi-turn resonator at scan rates from 4.32 to 43.2 kG/s were deconvolved. The resulting spectra were compared with each other and with slow-scan lineshapes. The deconvolution procedure also was shown to give good results for signals in the presence of gradients of various magnitudes for a phantom consisting of two LiPc samples separated by 5 mm.

### 2.9. Imaging

A 2D spectral-spatial image of a phantom consisting of two LiPc samples and a 0.5 mM trityl sample was reconstructed from projections collected with the 25 mm multi-turn resonator and magnet Assembly II. The distance between the two LiPc samples was ~5 mm and the distance between the middle LiPc sample and the center of the trityl sample was ~8 mm. Sixty experimental projections out of a complete set of 64 projections were obtained at a scan frequency of 8 kHz and scan widths of 1.3–9.72 G. Gradients (6.7 mG/cm to 2.2 G/cm) were applied in the $Z$ direction. The resulting rapid-scan signals were deconvolved and the image was reconstructed by filtered back-projection using the missing angle algorithm described in [28,29] and implemented in a locally written program in Compaq Visual Fortran 6.5.

## 3. Results and discussion

Rapid-scan signals for 0.2 mM trityl in a 4 mm OD tube were obtained using the 4 mm multi-turn resonator (Fig. 1). Unlike traditional slow-scan EPR, the direct-detection rapid-scan EPR experiment does not use phase-sensitive detection and records the absorption signal directly instead of the derivative of the absorption signal. The locally built triangular scan driver was used to generate scan rates between 1.76 and 30.0 kG/s. The spectrum recorded at 1.76 kG/s (Fig. 1A) closely resembles the integral of the first-derivative slow-scan spectrum (not shown). The $^{13}C$ hyperfine lines with $a_H = 0.166$ G are resolved on each side of the signal. As the scan rate is increased, oscillations that are characteristic of rapid-scan conditions appear on the trailing edge of the signal, the signal broadens, and the peak shifts to the right. The $^{13}C$ hyperfine lines that were seen

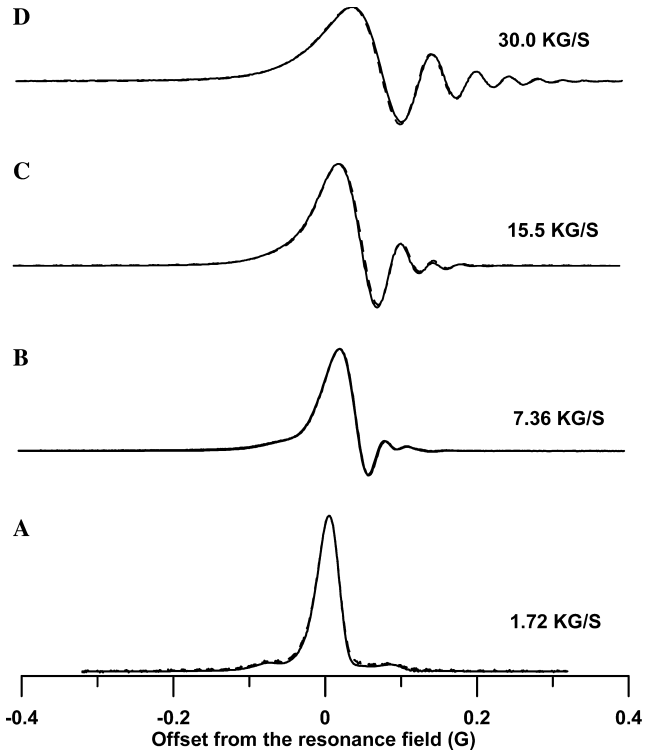


Fig. 1. Rapid-scan signals for a 0.2 mM aqueous trityl solution obtained at an RF frequency of 248 MHz and $B_1 = 6.4$ mG. The signals were recorded using (A) scan frequency, 1.34 kHz; scan width, 0.64 G; and scan rate, 1.72 kG/s. (B) Scan frequency, 2 kHz; scan width, 1.84 G; and scan rate, 7.36 kG/s. (C) Scan frequency, 4.2 kHz; scan width, 1.85 G; and scan rate; 15.5 kG/s. (D) Scan frequency, 8.1 kHz; scan width, 1.85 G; and scan rate, 30.0 kG/s. The solid lines are the experimental data and the dashed lines are the simulations. The scale on the $x$ axis is the offset in Gauss from the center of the scan.

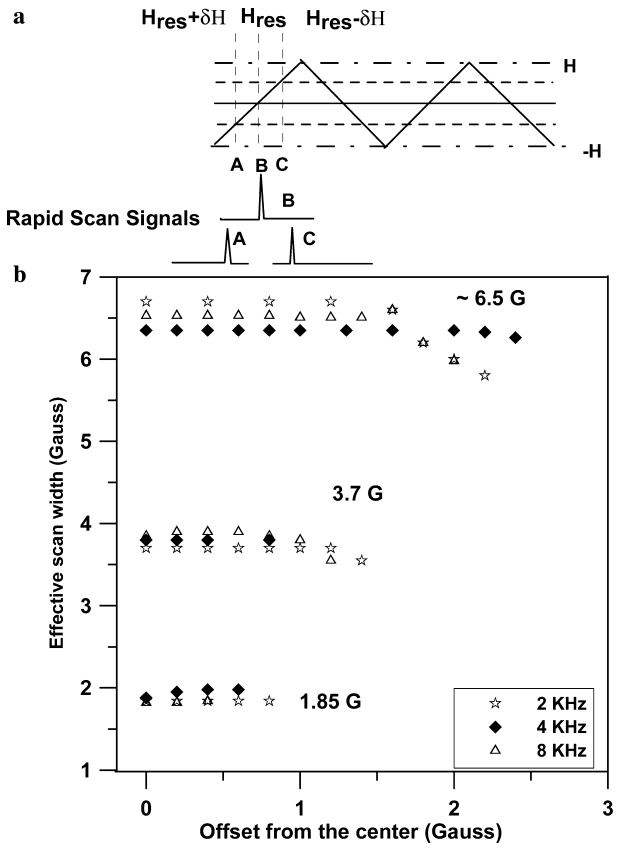


Fig. 2. (a) Scheme for testing the linearity of the triangular scan. During a half-cycle the magnetic field is scanned from −H to +H relative to center field. Points B, A, and C represent settings of the center field that cause the observed signal to be offset in the scan. (b) Effective scan widths for various scan frequencies and scan widths plotted as a function of the offset in the dc field. The data were recorded using the 4 mm multi-turn resonator at an RF frequency of 253 MHz and with $B_1 = 6.4$ mG.

in the signals recorded at scan rates of 1.72 kG/s (Fig. 1A) and 7.36 kG/s (Fig. 1B) are not resolved at faster scan rates. There is good agreement between experimental and simulated curves.

As shown in Fig. 1, the shape of the rapid-scan signal is strongly dependent on scan rate. Fig. 2a illustrates how the center field was varied to position the signal at differing points in the scan and thereby use the signal lineshapes to test the linearity of the triangular scans. When the dc field is equal to the resonance field ($H_{res}$), the rapid-scan signal is observed at the center of the triangular scan (point B in the illustration). The signal can be shifted left or right in the scan by offsetting the dc field away from the resonance field ($H_{res} \pm \delta H$, points A and C in the illustration). For a linear (triangular) field scan, the scan rate (scan frequency times scan width times 2) remains constant throughout the half-cycle. In the simulations scan frequencies measured using a frequency counter were held constant and scan widths were adjusted to match simulated signals with experimental data obtained at various points in the half-cycle. An ~1% change in the scan width gave a detectable change in lineshape. Variations in the effective scan widths required to simulate the signals reflect deviations from linearity of the scan. The effective scan widths at various positions in the triangular scan that were determined by simulations of the signals are shown in Fig. 2b for various scan widths and scan frequencies. At a scan frequency of 4 kHz and scan widths of 1.85, 3.7, or 6.5 G and for the 1.85 G scan width at frequencies of 2 or 8 kHz the effective scan width remains nearly constant up to about 80% of the scan. The decrease in the effective scan width at the extremes of the scan indicates a "rounding" of the triangular scan that decreases the scan rate. At scan frequencies of 2 and 8 kHz and scan width of 6.5 G, the effective scan widths (rates) are constant up to about 70% of the scan above which there is an ~8% decrease. At a scan width of 3.7 G and scan frequency of 2 or 8 kHz, there is an ~5% decrease in the effective scan width at 65% of the scan. These observations indicate that for these scan widths and frequencies up to about 70% of the scan width is sufficiently linear that reliable spectroscopic information can be obtained.

As an additional test of the accuracy of the scan widths $^{13}C$ hyperfine splittings were measured from the rapid-scan spectra. Based on a CW experiment at X band the $^{13}C$ hyperfine splittings are 0.166, 1.27, 2.39, and 3.36 G. The rapid-scan signals are recorded on a time axis that can be converted to a magnetic field axis based on the known scan frequency and scan width. The hyperfine splittings calculated from the rapid-scan spectra were in good agreement with the X-band values.

The experimental and deconvolved rapid-scan signals for LiPc at various scan rates are shown in Fig. 3. Data were obtained using the 25 mm multi-turn resonator with a scan width of 2.16 G and scan frequencies from 1 to 10 kHz. The deconvolution process removes the oscillations and signal broadening caused by the rapid scan and restores the correct position of the peak maximum. To test the accuracy with which the slow-scan lineshape can be recovered from the rapid-scan signals, the deconvolved spectra shown in Fig. 3 are superimposed on the slow-scan spectrum in Fig. 4. The spectra demonstrate that the slow-scan lineshape can be restored very well for scan rates ranging from 4.32 to 43.2 kG/s.

The rapid-scan signals for two LiPc samples recorded in the presence of magnetic field gradients in the $Z$-direction are shown in Fig. 5. As the gradient is increased the

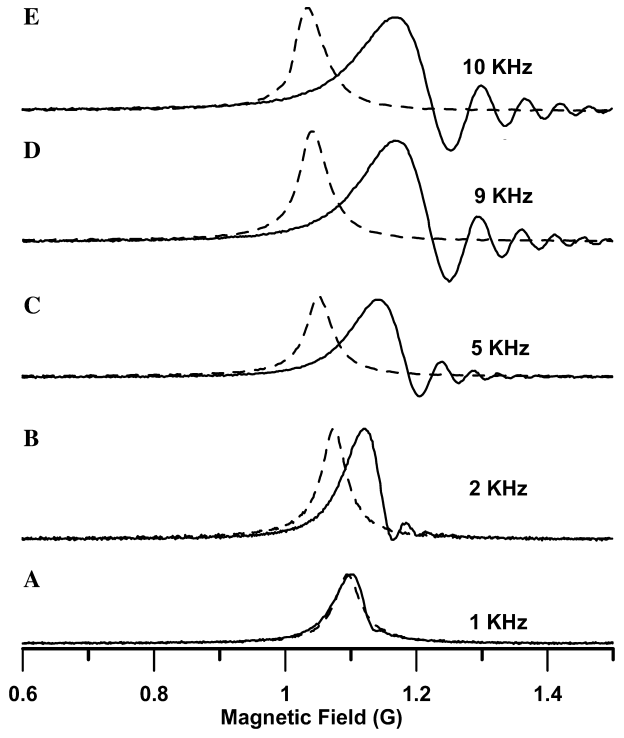


Fig. 3. Rapid-scan signals (solid lines) for a LiPc sample, obtained at RF frequency = 248 MHz and $B_1 = 3.6$ mG at various scan frequencies and the signals obtained by deconvolving these signals (dashed lines). The signals are obtained at various scan frequencies and a scan width of 2.16 G. The central segment of each scan is plotted. The corresponding scan rates (A–E) are 4.32, 8.64, 21.6, 38.8, and 43.2 kG/s.

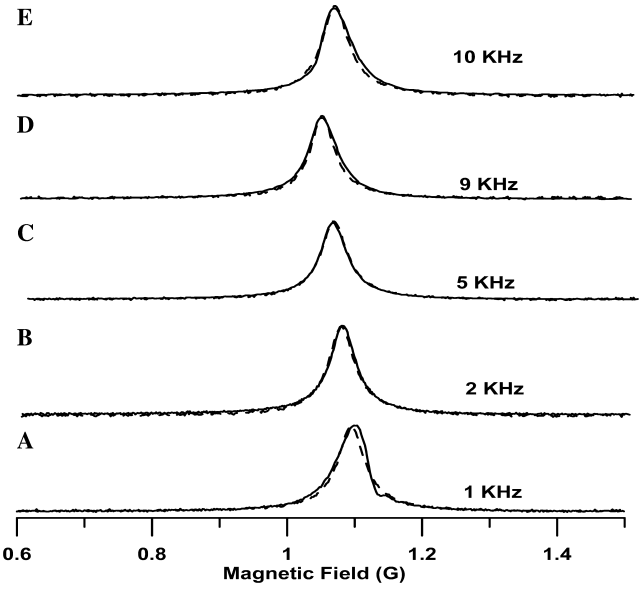


Fig. 4. (A) Experimental data obtained at a low scan rate (scan frequency, 1 kHz; scan width, 2.16 G) (solid line) and the deconvolved spectrum (dashed line). (B–E) Deconvolved spectra (dashed line) at 1 kHz shown in (A) superimposed on the spectra (solid lines) obtained by deconvolving the rapid-scan signals at higher scan rates. The deconvolved spectra in this figure are the same as in Fig. 3. The corresponding scan rates (A–E) are 4.32, 8.64, 21.6, 38.8, and 43.2 kG/s.

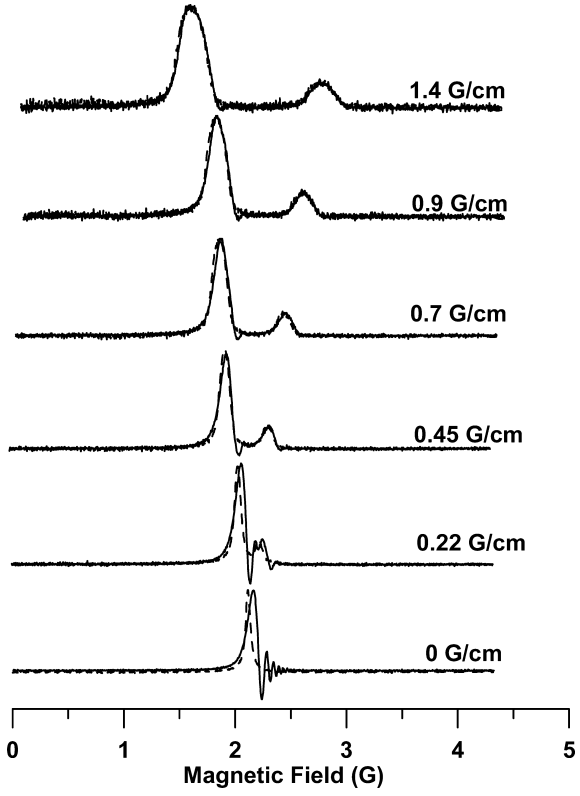


Fig. 5. Rapid-scan signals for two LiPc samples separated by ~5 mm, obtained in the presence of magnetic field gradients with RF frequency = 248 MHz, $B_1 = 2.6$ mG, and a scan frequency of 4 kHz. The solid lines are the experimental data and the dashed lines are deconvolved spectra.

separation between the signals from the two samples increases proportional to the physical separation between the samples, the signals broaden, and signal amplitudes decrease. At higher gradients the oscillations in the rapid-scan signals are damped due to the increased field inhomogeneity over the dimensions of the sample. The deconvolved spectra (dashed lines) agree well with the experimental signals (solid lines), which shows that deconvolution does not introduce distortions into the gradient-broadened spectra.

The inverse of the amplitude of the rapid-scan signals is plotted as a function of gradient in Fig. 6. The signal amplitude decreases approximately linearly with gradient. This behavior is in marked contrast to the behavior of signal amplitude in conventional CW spectra. In slow-scan spectroscopy with phase sensitive detection at the modulation frequency, the first derivative of the absorption signal is recorded, and the signal amplitude decreases quadratically with the field gradient. Unless additional signal averaging is performed, noise at constant bandwidth is independent of gradient so a decrease in signal causes a decrease in S/N. We propose that the weaker dependence of signal amplitude on gradient for the direct-detected signals will be a substantial advantage in imaging experiments. For example, projections for spectral–spatial images are recorded at a series of gradients and the quality of the reconstructed images is strongly dependent on the S/N for the projections at highest gradients.

A 2D spectral–spatial image of a phantom consisting of 2 LiPc samples and a 0.5 mM trityl sample is shown in Fig. 7. Fig. 7A is a cartoon of the phantom. The direction of the field gradient with respect to the sample geometry is shown by the arrow. Fig. 7B is the perspective plot of the image showing two strong peaks due to the LiPc samples and a weaker peak due to the trityl sample. Fig. 7C is the contour plot of the same image. For the lengths of the spectral and spatial dimensions selected for this image, the localized LiPc samples give rise to circularly symmetric regions in the 2D spectral–spatial plane. The 0.5 mM trityl sample, which has a greater

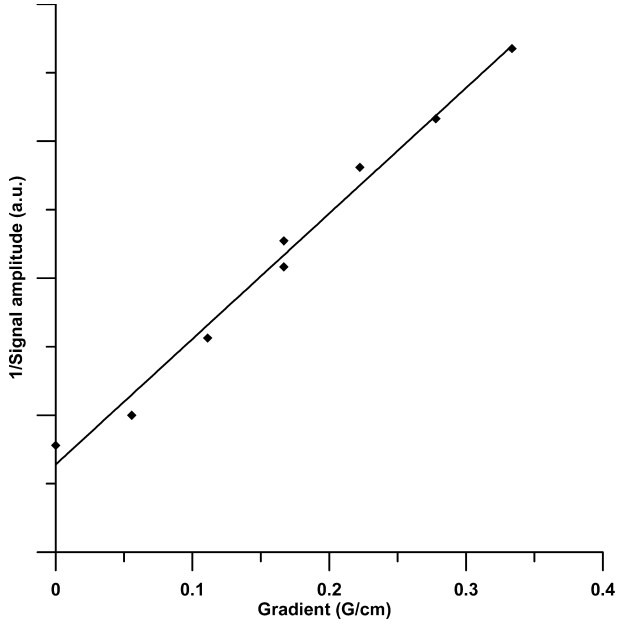


Fig. 6. Dependence of the reciprocal of the signal amplitude on the magnetic field gradient. The solid line shows the linear fit.

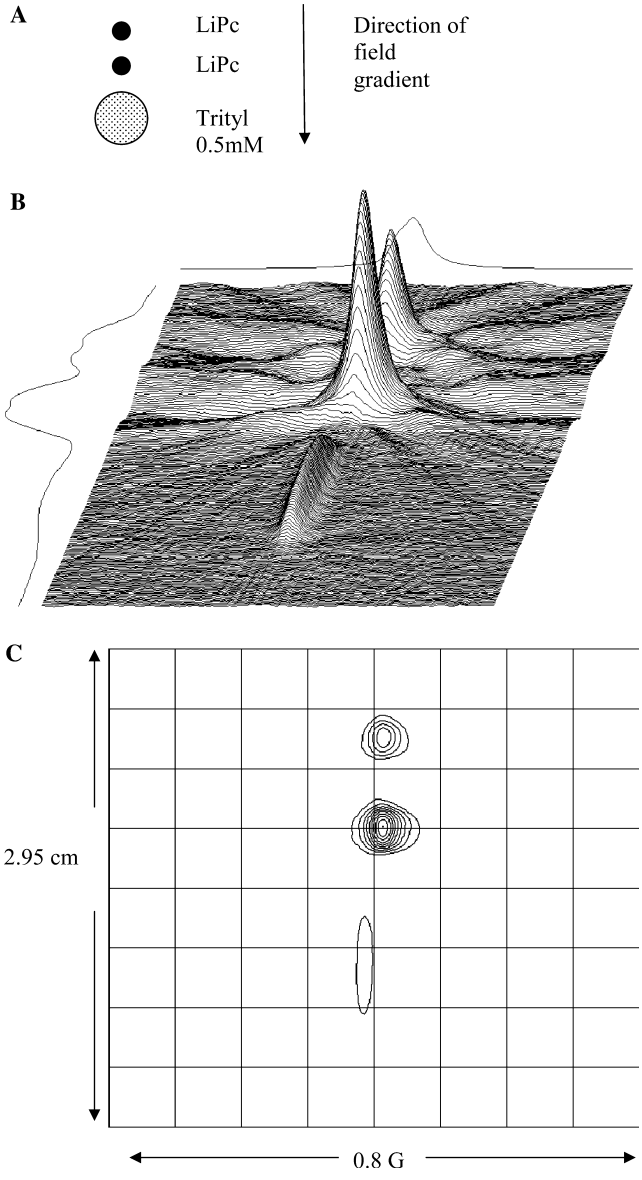


Fig. 7. (A) A cartoon of the phantom consisting of two LiPc samples and a 0.5 mM trityl sample. The separations between centers of tubes are ~5 mm and ~8 mm, respectively. The direction of the field gradients is shown by the arrow. (B) Perspective plot of the 2D spectral–spatial image of the phantom obtained by rapid-scan at 8 kHz. The RF frequency was 248 MHz and $B_1$ was 3.6 mG. (C) Contour plot of the image showing circularly symmetric contours corresponding to the LiPc samples and a much less intense elongated contour due the trityl sample. On the spectral axis, the contour due to the trityl sample is displaced relative to the contours due to the LiPc samples by ~0.03 G, consistent with the difference in $g$ values. The lowest contour is 15% of maximum.

spatial extent (8 mm inner diameter of the quartz tube) gives rise to a contour that is elongated along the spatial axis. The separation between the contours matches well with the actual separation between the samples in the phantom. On the spectral axis, the contour due to the trityl sample is displaced by ~0.03 G with respect to the LiPc contours. This difference in the resonance positions between LiPc and trityl reflects a difference in the $g$ values of the two samples. The full widths at half-maximum of 49 mG for the LiPc peak and 37 mG for the trityl peak measured from spectral slices of the image agree well with non-gradient spectra of the two species.

## 4. Conclusions

A triangular scan current driver permits direct-detected rapid-scan EPR signals to be recorded at scan rates up to about 60 kG/s with good linearity over 70–80% of the scan widths. The resulting rapid-scan EPR signal can be Fourier deconvolved using an analytical function to recover lineshapes that agree well with spectra recorded at slow scan rates. The deconvolution procedure also works well in the presence of magnetic field gradients. The spectral lineshapes and spatial dimensions in a 2D spectral–spatial image reconstructed from deconvolved projections are in good agreement with known properties of the sample.

## Acknowledgments

Financial support from National Institutes of Health NIBIB EB000557 is gratefully acknowledged. Professor Harold Swartz, Dartmouth University, graciously provided LiPc that was prepared with funding from NIBIB EB002180 for the EPR Center for the Study of Viable Systems. The trityl-$CD_3$ radical was a generous gift from Nycomed Innovations AB to Professor Howard Halpern, University of Chicago, who supplied it for this study, as a collaborative project under NIBIB EB002034 for the Center for EPR Imaging in vivo Physiology.

## References

[1] N. Bloembergen, E.M. Purcell, R.V. Pound, Phys. Rev. 73 (1948) 679–712.
[2] B.A. Jacobsohn, R.K. Wangness, Phys. Rev. 73 (1948) 942.
[3] J.I. Kaplan, J. Chem. Phys. 57 (1972) 5615–5616.
[4] J.I. Kaplan, J. Chem. Phys. 59 (1973) 990.
[5] R.R. Ernst, J. Chem. Phys. 59 (1973) 989.
[6] J. Dadok, R.F. Sprecher, J. Magn. Reson. 13 (1974) 243–248.
[7] R.K. Gupta, J.A. Ferretti, E.D. Becker, J. Magn. Reson. 13 (1974) 275–290.
[8] R.K. Gupta, J.A. Ferretti, E.D. Becker, J. Magn. Reson. 16 (1974) 505–507.
[9] D. Shaw, Specialist Periodical Reports, Nucl. Magn. Res. 5 (1976) 188–204.
[10] Y. Arata, H. Ozawa, J. Magn. Res. 21 (1976) 67–76.
[11] H. Ozawa, Y. Arata, Chem. Lett. (1975) 239–240.
[12] Y. Arata, H. Ozawa, Chem. Lett. (1974) 1257–1260.
[13] H. Akutsu, Y. Kyogoku, I. Kagawa, Bull. Chem. Soc. Jpn. 53 (1980) 904–907.
[14] T. Ogino, Y. Arata, S. Fujiwara, J. Magn. Res. 39 (1980) 381–389.
[15] H. Ozawa, Y. Arata, Bull. Chem. Soc. Jpn. 55 (1982) 411–414.
[16] J. Jen, J. Magn. Res. 45 (1981) 257–269.
[17] P.S. Belton, in: D.N. Rutledge (Ed.), Signal Treatment and Signal Analysis in NMR, Elsevier, Amsterdam, 1996.
[18] G.A. Morris, H. Barjat, T.J. Horne, J. Prog. Nucl. Magn. Reson. Spectros. 31 (1997) 197–257.
[19] J.W. Stoner, D. Szymanski, S.S. Eaton, R.W. Quine, G.A. Rinard, G.R. Eaton, J. Magn. Res. 170 (2004) 127–135.
[20] S.K. Rengan, V.R. Bhagat, V.S.S. Sastry, B. Venkataraman, J. Magn. Reson. 33 (1979) 227–240.
[21] R. Czoch, J. Duchiewicz, A. Francik, S. Indyka, J. Koscielniak, Meas. Automatic Control 29 (1983) 41–43.
[22] J.P. Joshi, G.R. Eaton, S.S. Eaton, Appl. Magn. Reson. (2005) (in press).
[23] P. Turek, J.J. Andre, A. Giraudeau, J. Simon, Chem. Phys. Lett. 134 (1987) 471–476.
[24] V.O. Grinberg, A.I. Smirnov, O.Y. Grinberg, S.A. Grinberg, J.A. O'Hara, H.M. Swartz, Appl. Magn. Reson. (2005) (in press).
[25] R.W. Quine, G.A. Rinard, S.S. Eaton, G.R. Eaton, Magn. Reson. Eng. 15 (2002) 59–91.
[26] G.A. Rinard, R.W. Quine, S.S. Eaton, G.R. Eaton, E.D. Barth, C.A. Pelizzari, H.J. Halpern, Magn. Reson. Eng. 15 (2002) 51–58.
[27] G.K. Wertheim, M.A. Butler, K.W. West, D.N.E. Buchanan, Rev. Sci. Instrum. 45 (1974) 1369–1371.
[28] M.M. Maltempo, S.S. Eaton, G.R. Eaton, J. Magn. Reson. 77 (1988) 75–83.
[29] G.R. Eaton, S.S. Eaton, K. Ohno, EPR Imaging and in Vivo EPR, CRC Press, Boca Raton, FL, 1991.